

# Dynamical aspects of isotopic scaling

Martin Veselsky

Institute of Physics, Slovak Academy of Sciences,  
Dubravská cesta 9, Bratislava, Slovakia  
e-mail: fyzimarv@savba.sk

## Abstract

Investigation of the effect of dynamical stage established that increasing width of initial isospin distributions is reflected by significant modification of the slope of final isoscaling plots after de-excitation. For narrow initial distributions, the slope of isoscaling plots assumes the limiting value for two individual initial nuclei while for wide initial distributions the slope for hot fragments approaches the initial value. The slopes of isoscaling plots for final cold fragments increase due to secondary emission. The experimentally observed evolution of the isoscaling parameter in the multifragmentation of hot quasiprojectiles at 50 A MeV, fragmentation of  $^{86}\text{Kr}$  beam at 25 A MeV and multifragmentation of target spectator at relativistic energies was reproduced by the simulation with dynamical stage described using the appropriate model ( deep inelastic transfer and incomplete fusion for Fermi energy domain and spectator-participant model for relativistic energies ) and de-excitation stage described using the statistical multifragmentation model. In all cases the isoscaling behavior was reproduced by proper description of the dynamical stage and no unambiguous signals of the decrease of the symmetry energy coefficient were observed.

## Introduction

The studies of multifragmentation in the recent years highlighted the importance of the fragment yield ratios which can be used to extract thermo-

dynamical observables of the fragmenting system such as temperature and chemical potential ( for review of related methods see e.g. [1] ). In the context of isotopic distributions, the fragment yield ratios represent the details of the distribution sensitive to isospin degrees of freedom. Similar sensitivity can be explored globally by investigating the ratio of isotopic yields from two processes with different isospin asymmetry, essentially dividing the two isotopic distributions in point-by-point fashion. When employing the macro-canonical formula for fragment yields, such a ratio will depend on  $N$  and  $Z$  as follows [2]

$$R_{21}(N, Z) = Y_2(N, Z)/Y_1(N, Z) = C \exp(\alpha N + \beta Z) \quad (1)$$

where  $\alpha = \Delta\mu_n/T$  and  $\beta = \Delta\mu_p/T$ ,  $\Delta\mu_n$  and  $\Delta\mu_p$  are the differences in the free neutron and proton chemical potentials of the fragmenting systems.  $C$  is an overall normalization constant. Alternatively [3] the dependence can be expressed as

$$R_{21}(N, Z) = Y_2(N, Z)/Y_1(N, Z) = C \exp(\alpha' A + \beta'(N - Z)) \quad (2)$$

thus introducing the parameters which can be related to the isoscalar and isovector components of free nucleon chemical potential since  $\alpha' = \Delta(\mu_n + \mu_p)/2T$  and  $\beta' = \Delta(\mu_n - \mu_p)/2T$ .

An exponential scaling of  $R_{21}$  with the neutron and proton numbers was observed experimentally in the multifragmentation data from the reactions of high-energy light particles with massive target nucleus [3, 4] or from the reactions of mass symmetric projectile and target at intermediate energies [2] and such behavior is called isotopic scaling or isoscaling [2] ( the parameters  $\alpha, \beta, \alpha', \beta'$  being called isoscaling parameters ). Isoscaling behavior was further reported in the heavy residue data [5] and also in fission data [6]. The values of isoscaling parameters were related by several authors to various physical quantities such as symmetry energy [2, 3], level of isospin equilibration [5] or the values of transport coefficients [6].

As demonstrated in the literature, isoscaling appears to be a global feature of the reaction and multifragmentation data and the values of isoscaling parameters show sensitivity to both dynamical and thermodynamical properties of the hot source created in the dynamical stage of the collision. It is of interest to clarify to which extent the isoscaling behavior is modified by the process of de-excitation and whether the dynamical and thermodynamical properties of the hot source can be disentangled.

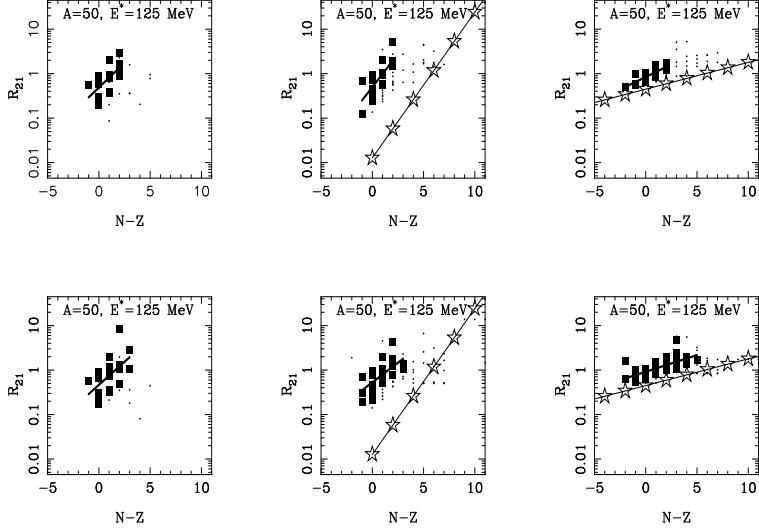


Figure 1: Isoscaling plots after de-excitation by the SMM for nuclei with mass  $A = 50$  and excitation energy 125 MeV. Upper and lower rows represent cold and hot partitions, respectively. Squares and thick solid lines - isoscaling plots and exponential fits for  $Z \leq 6$ , scattered dots - all  $Z$ 's. Dynamical stage ( stars connected by thin solid lines ) was simulated by shifted Gaussians (  $N/Z = 1.0, 1.3$  ) with three different values of widths (  $\sigma_Z = 0.5, 2.5, 4.5$  , see panels from left to right ).

## Effect of the de-excitation stage on isoscaling

To disentangle dynamical and thermodynamical properties of the hot source in the experimental data and specifically to determine the isoscaling properties after the dynamical stage one can perform simulation of the de-excitation process for various initial isospin distributions which can be produced in the dynamical stage, thus allowing to establish the relation between isoscaling behavior prior to and after de-excitation. In the present work the de-excitation stage is simulated using the de-excitation code SMM [7], representing the combination of statistical multifragmentation model ( SMM ) for highly excited nuclei with evaporation/fission cascade for lower excitation energies. The reaction simulations which used the SMM for the de-excitation stage proved consistently better than using the model of sequential binary decay, especially for the neutron-rich nuclides [8] and residues after de-excitation of hot nuclei [9]. Some discrepancies were observed for the yields of a limited

set of the  $\beta$ -stable nuclei [8] close to the projectile, which were overestimated due to low probability for emission of complex fragments below multifragmentation threshold [9].

The effect of the de-excitation stage was investigated for initial ( dynamical ) isobaric distributions with three masses  $A = 25, 50, 100$ , thus covering the typical mass range where the multifragmentation studies are performed. In the nuclear reactions, the de-excitation stage is preceded by the dynamical stage where the hot nuclei are formed. An open question is how the isoscaling behavior looks after dynamical stage and to what extent it is modified by the process of de-excitation. A possible way to answer such question is to generate the distributions of hot nuclei exhibiting isoscaling and to observe the effect of de-excitation. In order to generate the initial dynamical distributions exhibiting isoscaling one can explore the well known fact that after dividing two Gaussian distributions with equal width and shifted centers, an exponential is obtained and thus isoscaling is guaranteed. The logarithmic slope of such dependence ( isoscaling parameter ) will thus be determined by the centers of two Gaussian distributions  $x_1, x_2$  and their common width  $\sigma$

$$\alpha = (x_2 - x_1)/\sigma^2 \quad (3)$$

and variation of the parameters of Gaussian distributions will allow to vary the initial isoscaling behavior. In the present work the positions of the centers are fixed and the Gaussian width is used to control isoscaling behavior. Such a choice reflects the situation in damped nucleus-nucleus collisions where the initial isospin asymmetry is not changed dramatically while the width of distribution evolves quickly with damping of initial kinetic energy. In the simulations presented here, the isoscaling after dynamical stage was simulated using initial elemental distributions approximated by two Gaussians with shifted centers (  $N/Z = 1.0, 1.3$  ). Three different values of common Gaussian width were used (  $\sigma_Z = 0.5, 1.5, 3.5$  for  $A = 25$  and  $0.5, 2.5, 4.5$  for  $A = 50, 100$  ). For each mass, the yields of final products were simulated with good statistics for hot sources with five selected atomic numbers and for other elements the yields of final products were estimated using polynomial interpolation. The calculation was carried out for two values of excitation energy 2.5 and 5.0 AMeV, the former representing the region of multifragmentation threshold while the latter corresponds to the region where multifragmentation is the main de-excitation mode.

In the Figs. 1, 2 are shown results for nuclei with mass  $A = 50$  and

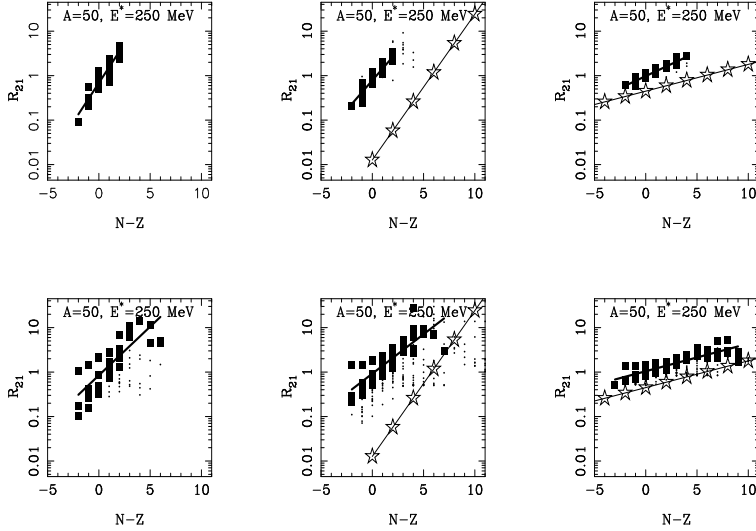


Figure 2: Isoscaling plots after de-excitation by the SMM for nuclei with mass  $A=50$  and excitation energy 250 MeV ( $\sigma_Z = 0.5, 2.5, 4.5$ ). Symbols and lines as in Fig. 1.

excitation energies 125 and 250 MeV. For the narrow initial distributions (left columns) the isoscaling plots appear to be governed by the intrinsic effect of de-excitation, while with increasing width (middle and right columns) the effect of initial distributions appears to take over. Secondary emission leads to slight increase of the slope due to lower temperature which, according to macro-canonical theory (Eqs. (1) and (2)), enters into denominator. For the widest initial distribution (right columns) the isoscaling plot in the hot partition appears to follow the initial isoscaling plot and increase of the slope by secondary emission determines the final discrepancy.

The results for nuclei with mass  $A = 25$  and excitation energies 63 and 125 MeV are shown in Figs. 3, 4. Analogous conclusions as for  $A = 50$  can be made, in this case the situation, where isoscaling plots for hot partitions follow the initial isoscaling and final discrepancy is determined by secondary emission, occurs for both middle and right panels and thus such asymptotic behavior takes over faster with increasing initial width.

The situation for  $A = 100$  (excitation energies 250 and 500 MeV) is shown in Figs. 5, 6. The behavior is analogous to previous cases, but the slope of the isoscaling plot of fragments with  $Z \leq 6$  for the hot partition at the widest initial distribution appears to be larger than initial one, apparently

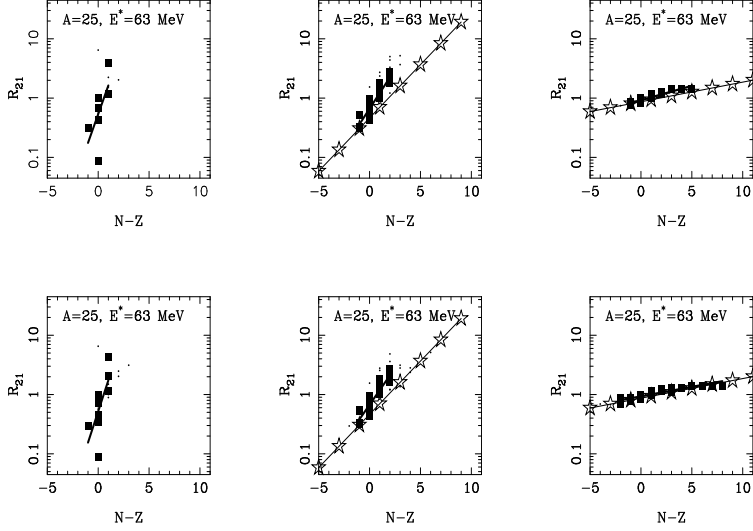


Figure 3: Isoscaling plots after de-excitation by the SMM for nuclei with mass  $A = 25$  and excitation energy  $63 \text{ MeV}$  ( $\sigma_Z = 0.5, 1.5, 3.5$ ). Symbols and lines as in Fig. 1.

since the very isospin-asymmetric nuclei are produced and the symmetry energy of such light nuclei increases quickly and thus increasingly influences the overall energy balance. However, for heavier fragments (dots) the isoscaling behavior appears to follow the initial distributions better. On the other hand, such sensitivity to symmetry energy for light fragments originating from hot heavy nuclei can in principle provide a probe of the symmetry energy coefficient at the hot stage, under assumption that reaction dynamics will lead to wide initial distributions and that it will be possible to reconstruct such initial distributions, possibly via full calorimetry of the hot source or via reliable simulations of the initial stage.

In general, increasing width of initial isobaric distributions (and corresponding decrease of the slope of initial isoscaling plots) is reflected by significant modification of the slope of final isoscaling plots after de-excitation. For narrow initial distributions, the slope of isoscaling plots assumes the limiting value corresponding to two individual initial nuclei which is fully determined by the details of their de-excitation. For wide initial distributions, the slope of isoscaling plots for hot fragments approaches the slope of initial isoscaling plots and is thus fully determined by initial stage. This correspondence is modified by secondary emission and the slopes of isoscaling plots for final

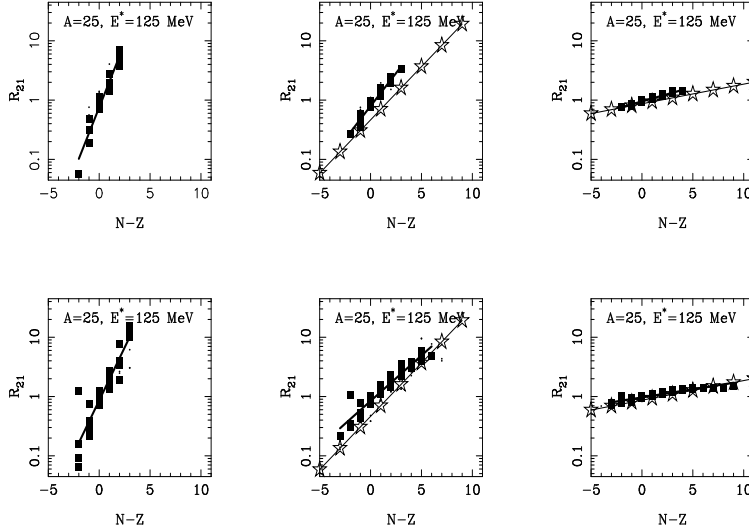


Figure 4: Isoscaling plots after de-excitation by the SMM for nuclei with mass  $A=25$  and excitation energy 125 MeV ( $\sigma_Z = 0.5, 1.5, 3.5$ ). Symbols and lines as in Fig. 1.

cold fragments are larger by the value possibly corresponding to lowering of temperature during secondary emission. It is noteworthy, that the width of initial Gaussian distributions causes the decrease of the isoscaling parameters comparable to the values, reported in the literature [2, 3] as an effect of the decrease of symmetry energy, according to liquid-drop based formula relating the coefficient of symmetry energy directly to the value of the isoscaling parameter. However, the effect of dynamical stage and specifically of the width of initial distributions was not considered in the analysis and the estimates are based on simulation for individual initial nuclei, which appears to be an overly simplified approach.

## Investigation of dynamical stage in selected reactions

Investigation of the effect of initial ( dynamical ) isospin distributions on isoscaling after de-excitation, presented in previous section, implies that the dynamical stage, leading to evolution of considerable width of isospin distribution, plays an important role in determination of the isoscaling behavior

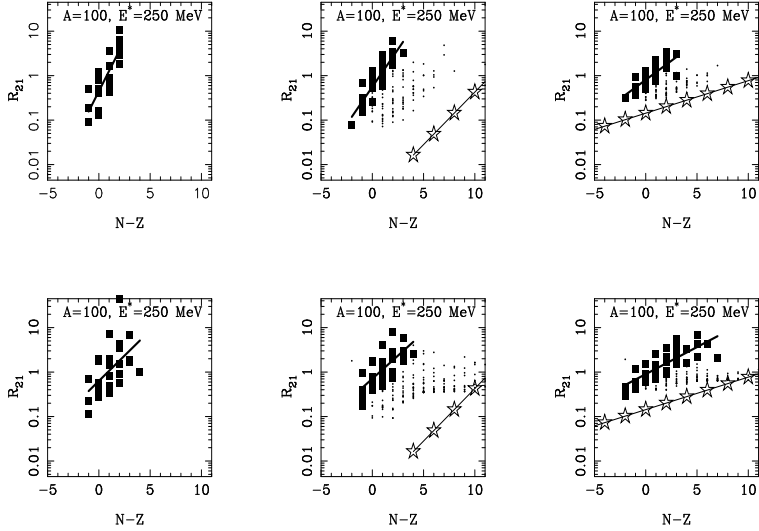


Figure 5: Isoscaling plots after de-excitation by the SMM for nuclei with mass  $A = 100$  and excitation energy 250 MeV ( $\sigma_Z = 0.5, 2.5, 4.5$ ). Symbols and lines as in Fig. 1.

of final products. Detailed understanding of reaction dynamics is thus necessary to allow disentangling the properties of hot multifragmentation source from the artifacts of the reaction dynamics. Selected cases ( multifragmentation of hot quasiprojectiles at 50 AMeV, fragmentation of  $^{86}\text{Kr}$  beam at 25 AMeV and multifragmentation of target spectator at relativistic energies ) will be presented in this section in order to investigate the effect of reaction dynamics on isoscaling behavior in few energy regions for hot nuclei with different masses.

## Multifragmentation of projectiles with $A \sim 25$ at projectile energies around the Fermi energy

The multifragmentation of hot quasiprojectiles with  $A \sim 25$  was investigated in reactions  $^{28}\text{Si} + ^{124,112}\text{Sn}$  at projectile energy 50 and 30 AMeV [10]. The observed fragment data [10] provide full information ( with exception of emitted neutrons ) on the decay of thermally equilibrated hot quasi-projectiles with known mass (  $A = 20 - 30$  ), charge, velocity and excitation energy.

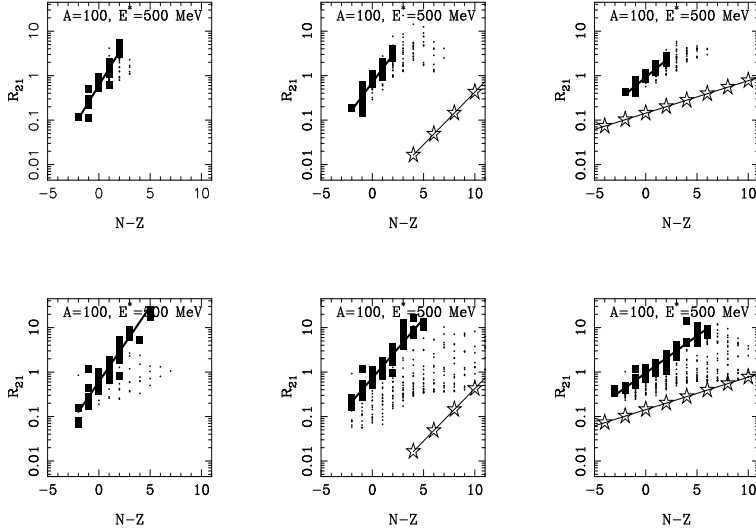


Figure 6: Isoscaling plots after de-excitation by the SMM for nuclei with mass  $A = 100$  and excitation energy 500 MeV ( $\sigma_Z = 0.5, 2.5, 4.5$ ). Symbols and lines as in Fig. 1.

Detailed investigation of the reaction mechanism [10] allowed to establish a dominant reaction scenario. Excellent description of the fragment observables was obtained using the model of deep-inelastic transfer (DIT) [11] for the early stage of collisions and the statistical multifragmentation model (SMM) [7] for de-excitation. The model describes well the dynamical properties of the reconstructed quasi-projectile such as center of mass velocity, excitation energy and isospin-asymmetry. The fragment observables such as multiplicity, charge distributions and mean values of  $N/Z$  for a given charge were also reproduced reasonably well [10]. Thus the data can be considered as well understood in terms of reaction mechanism. The contribution from non-equilibrium processes such as pre-equilibrium emission was shown to be weak [10]. According to successful DIT+SMM simulation, the number of emitted neutrons, which are not detected, was between one and two per event and the underestimation of the excitation energy by the evaluated apparent excitation energy due to neutron emission can be expected approximately 10–15 % in the wide range of excitation energies. The excitation energy dependence of the isoscaling parameter, corrected for the  $1/T$  temperature dependence, exhibits a turning-point at 4 AMeV [12] which can be interpreted as a signal of the onset of separation into isospin asymmetric

dilute and isospin symmetric dense phase. The onset of chemical separation is correlated to the onset of the plateau in the caloric curve, thus signaling that chemical separation is accompanied by a latent heat.

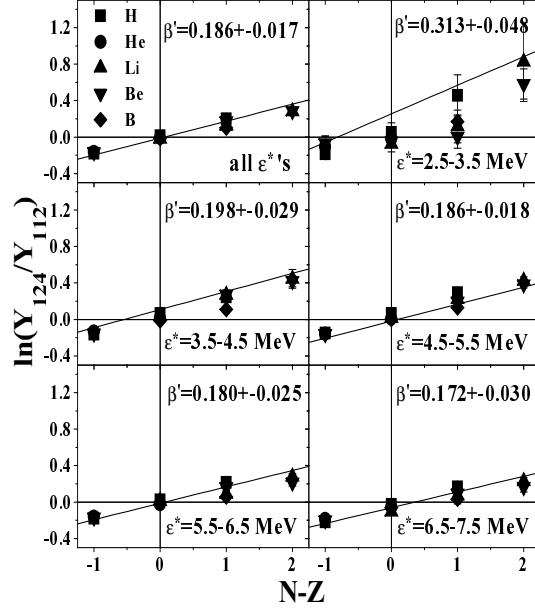


Figure 7: Simulated isoscaling plots ( symbols ) and fits to experimental data ( lines ) from statistical decay of hot quasiprojectiles from the reactions  $^{28}\text{Si}+^{124,112}\text{Sn}$  at projectile energy 50 AMeV for inclusive data and five excitation energy bins.

In Fig. 7 are presented simulated isoscaling data ( symbols ) from statistical decay of hot quasiprojectiles from the reactions  $^{28}\text{Si}+^{124,112}\text{Sn}$  at projectile energy 50 AMeV. The isoscaling plots are presented not only for the inclusive data but also for five bins of excitation energy. The slope depends on the excitation energy almost identically as in experiment, which is represented by solid lines, corresponding to exponential fits of experimental data. The DIT+SMM simulation fully reproduces experimental isoscaling behavior. Concerning the reaction dynamics, the isoscaling parameters of initial isospin distributions exhibit similar trend as the final values, in agreement with the results of simulation presented in Figs. 3, 4. The shift between simulated initial isospin distributions is constant for all excitation energy bins and the evolution is essentially determined by the widths which are lower at lowest excitation energy bins and then depend on excitation energy only

weakly. Despite overall success of simulation it does not allow to extract unambiguously the values of the temperature corresponding to isospin trends of hot fragment distributions, due to the fact that production of multiple fragments occurs at most part in secondary emission represented by Fermi decay. The formalism of Fermi decay is analogous to multifragmentation model with cold fragment partition, which thus essentially duplicates the multifragmentation model with hot fragments used in the SMM. Thus the model does not provide an unambiguous equivalent to experimental double-isotope ratio or slope temperatures, used in [12, 13]. The duplicity of fragmentation stages in the calculation is consistent with the analogous success of the model of sequential binary decay for light nuclei, where the proper exploration of available phase space appears a most important requirement to the successful model.

## Fragmentation of $^{86}\text{Kr}$ beam with tin targets at 25 AMeV

The isoscaling phenomena are not restricted to relatively light fragments ( compared to the mass of the composite system ) but can be observed in heavy residue data, measured at zero angle. Yield ratios  $R_{21}(A, Z)$  of projectile residues from the reactions of  $^{86}\text{Kr}$  ( 25 AMeV ) with  $^{124,112}\text{Sn}$  [14] were investigated and it was observed that the ratios for each isotopic ( isotonic ) chain exhibit isoscaling behavior. The slopes are constant for fragment mass range  $A = 25 - 60$ , corresponding to primary events with the maximum observed excitation energy of 2.2 AMeV. For heavier fragments, the slopes exhibited gradual decrease with increasing mass of the fragments. Assuming that the fragmentation occurs at normal density, using  $C_{sym} = 25$  MeV [3], the values of isoscaling parameters can be used to determine the values of  $\Delta(N/Z)_{qp}$  as a function of the observed fragment mass  $A$  ( charge  $Z$  ), thus demonstrating the evolution of the  $N/Z$  equilibration process in the isospin-asymmetric collisions. The monotonic increase of  $\Delta(N/Z)_{qp}$  with excitation energy can be understood as a result of the mechanism of nucleon exchange.

In the left panel of Fig. 8 are shown isoscaling plots of the simulated data for the reactions of  $^{86}\text{Kr}$  (25AMeV) with  $^{124,112}\text{Sn}$ . The simulation used is the same as in [16] where it allowed to reproduce experimental cross sections for the neutron-rich nuclides and residues from de-excitation of hot nuclei. Some discrepancies were observed for the yields of a limited set of the  $\beta$ -stable nuclei close to the projectile, which were overestimated due to low probability

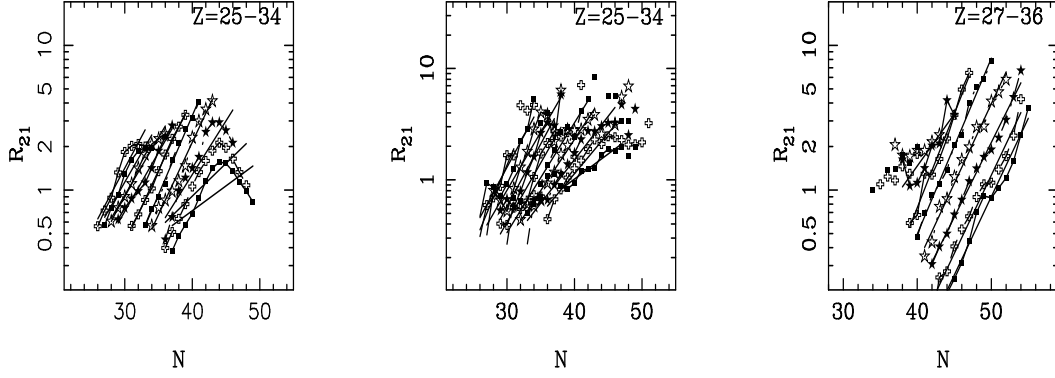


Figure 8: Isoscaling plots for the reactions of  $^{86}\text{Kr}$  (25A MeV) with  $^{124,112}\text{Sn}$ . Left panel - simulated data for final fragments, middle panel - experimental data [15], right panel - simulated data after dynamical stage. Lines represent exponential fits.

for emission of complex fragments below multifragmentation threshold. For comparison, in the middle panel are shown experimental isoscaling plots. For nuclei with  $Z=25-30$  the simulation and experiment lead to similar behavior with constant slopes and compatible values of isoscaling parameters. For lower  $Z$ 's ( $Z \leq 24$ , not shown in the Fig. 8) the experimentally observed slopes become even larger than the calculated ones, thus eventually implying a physical phenomenon not considered in simulations, however this effect can be caused by experimental limitations for the observed yields of these elements in the tails of isotopic distributions (as discussed in [16]) leading to lower widths of isotopic distributions and thus larger apparent values of isoscaling parameters. For heavier nuclei with  $N > 44$ , the simulation leads to reverse trend of the yield ratio toward unity, thus possibly signaling an onset of reaction mechanism independent of the target isospin, possibly quasi-elastic (direct) few-nucleon transfer taking place at very peripheral collisions. The experimental isoscaling behavior for these nuclei shows signs of similar reverted trend, the transition is not as regular as in the simulation and the inclusion of the points from this region into exponential fits (lines) leads to decrease of apparent slopes of isoscaling plots. Similar decrease of the slope of exponential ("isoscaling") fits is suggested by the lines in the left panel, despite very poor quality of such fits. Thus the evolution of the apparent slopes of exponential plots in both experimental and simu-

lated data suggest a mixing of two components, one very sensitive to target isospin, possibly intense nucleon exchange, while the second one, quasi-elastic few-nucleon exchange, is almost insensitive. The situation is demonstrated in the right panel where simulated isoscaling plots are shown for dynamical stage prior to de-excitation. The isotopes with  $Z = 30 - 36$  exhibit regular isoscaling behavior, except for a structure around  $N = 50$  for elements close to projectile, which can be identified with quasi-elastic processes. Despite minor effect on isoscaling plots, these points represent a significant portion of reaction cross sections and corresponding wide excitation energy distribution leads to mixing with data for lighter elements and thus to modification of their isoscaling behavior after de-excitation. The discrepancy of final simulated and experimental isoscaling behavior can be possibly attributed to underestimated probability for emission of complex fragments below multi-fragmentation threshold in the SMM.

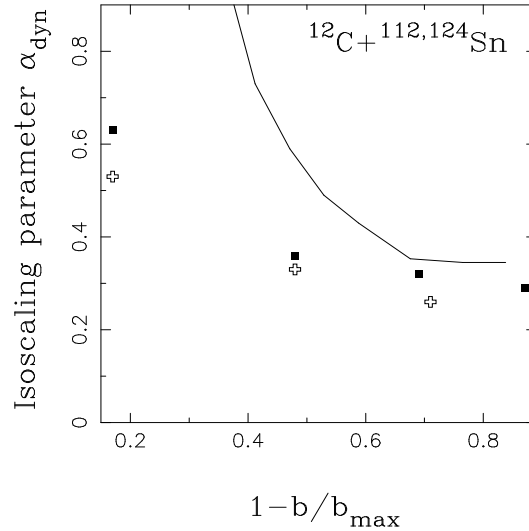


Figure 9: Evolution of the isoscaling parameter at dynamical stage as a function of centrality for the reactions  $^{12}\text{C} + ^{112,124}\text{Sn}$  at relativistic energy. Solid line - result of simulation, symbols - experimental data [17].

## Multifragmentation of target spectator at relativistic energy

The dominant reaction scenario at the relativistic energies is the spectator-participant scenario where the hot region is formed in the participant zone ( zone of geometric overlap ) while the spectator zones are relatively colder. Nevertheless, the spectator zones can be hot enough to undergo multifragmentation. The isoscaling behavior in the multifragmentation of target spectator was investigated in several works [4, 17] and the dependence of isoscaling parameter on centrality was observed [17]. The value of isoscaling parameter was related to symmetry energy [2, 3] and the decrease of the coefficient of symmetry energy was reported [17]. However, based on the conclusions of previous section, the effect of the reaction dynamics, specifically of the evolving width of mass and charge distributions, can be considered as an alternative interpretation. The volume and thus the most probable mass  $A_{TS}^{abr}$  of the target spectator can be estimated using the model of geometrical abrasion [18] as a function of the impact parameter. The number of nucleons in the spectator zone  $A_{TS}$  then can be estimated according to the binomial distribution

$$P(A_{TS}) = \binom{A_T}{A_{TS}} \left( \frac{A_{TS}^{abr}}{A_T} \right)^{A_{TS}} \left( 1 - \frac{A_{TS}^{abr}}{A_T} \right)^{A_T - A_{TS}} \quad (4)$$

where  $A_T$  is the target mass number. The charge of the spectator  $Z_{TS}$  can be determined as [19]

$$P(Z_{TS}) = \frac{\binom{Z_T}{Z_{TS}} \binom{N_T}{N_{TS}}}{\binom{A_T}{A_{TS}}} \quad (5)$$

where  $Z_T$  is the target mass number and  $N_{TS}$ ,  $N_T$  are neutron numbers of the target spectator and the target, respectively. The excitation energy of the target spectator can be, according to [20], estimated as proportional to the number of abraded nucleons with the proportionality factor 27 MeV, which was found to be consistent with experimental data [21].

Fig. 9 shows evolution of the isoscaling parameter after dynamical stage ( solid line ), obtained using centers and widths of simulated fragment distributions from the above calculation, as a function of centrality for the reactions  $^{12}\text{C} + ^{112,124}\text{Sn}$  at relativistic energies. Symbols show the experimental points reported in [17] for energy 300 and 600 AMeV. The calculation is capable

to reproduce the experimental trend without assumption on the decrease of the symmetry energy coefficient. The discrepancy at low centrality ( excitation energy ) can be explained by the asymptotics of the experimental points ( after de-excitation stage ) for the width approaching zero where the isoscaling parameter assumes a value determined by intrinsic properties of de-excitation. In the central collisions the isoscaling parameter exhibits analogous saturation at somewhat higher value ( by 10 - 15 % ) than reported in the experiment. The calculated widths of the target spectator isospin distributions at saturation are similar to the situation in the middle panel of Figs. 5, 6, where the initial ( dynamical ) isoscaling parameter reflects the initial value with remaining discrepancies due to secondary emission. In the present case the excitation energy exceeds 11 AMeV and the effect of secondary emission on the slope parameter in the test calculations was at the level of statistical errors ( not exceeding 10 % ). Thus after taking secondary emission into account the discrepancy will raise to the level of about 20 %, resulting in the corresponding decrease of the apparent symmetry energy coefficient from 25 MeV to about 20 MeV. Such a decrease is comparable with uncertainty in the choice of initial value of the symmetry energy coefficient in the models of nuclear ground state properties ( with the value of 23 MeV being commonly used ). The decrease of apparent symmetry energy coefficient can be further caused by other dynamical phenomena not included in the model such as emission at pre-equilibrium stage ( leading to decrease of the shift between the centroids and to additional increase of the widths of isotopic distributions ). The apparent value of the symmetry energy coefficient around 20 MeV can thus hardly be interpreted as a signal of significant decrease of the nuclear symmetry energy, in any case it is much less significant than it was reported in [17] ( up to factor of 6 after taking into account secondary emission ), where however the effect of dynamical evolution of initial isotopic distributions ( width in particular ) was not considered. The model description of the dynamical evolution presented here thus allows to reproduce the reported discrepancy almost fully, with the remaining discrepancy of the apparent symmetry energy coefficient not significant enough to be declared as an unambiguous signal.

## Summary and conclusions

Investigation of the effect of dynamical stage established that the increasing width of initial isospin distributions is reflected by significant modification of the slope of final isoscaling plots after de-excitation. For narrow initial distributions, the slope of isoscaling plots assumes the limiting value for two individual initial nuclei which is fully determined by the details of de-excitation. For wide initial distributions, the slope of isoscaling plots for hot fragments approaches the slope of initial isoscaling plots and is thus fully determined by initial stage. This correspondence is modified by secondary emission and the slopes of isoscaling plots for final cold fragments are larger by the value possibly corresponding to lowering of temperature during secondary emission. The decrease of the isoscaling parameters, caused by the increase of the width of initial Gaussian distributions, is comparable in magnitude to the values, reported in the literature as an effect of the decrease of the symmetry energy. The experimentally observed evolution of the isoscaling parameter in the statistical decay of hot quasiprojectiles from the reactions  $^{28}\text{Si}+^{124,112}\text{Sn}$  at projectile energy 50 AMeV is reproduced by the simulation with dynamical stage described using the model of deep inelastic transfer and de-excitation stage described using the statistical multifragmentation model. The evolution of the apparent slopes in both experimental and simulated data for projectile residues from the reactions of  $^{86}\text{Kr}$  ( 25 AMeV ) with  $^{124,112}\text{Sn}$  suggest a mixing of two components, one sensitive to target isospin, possibly intense nucleon exchange, while the second one, quasi-elastic few-nucleon exchange, almost insensitive. The discrepancy of final simulated and experimental isoscaling behavior can be possibly attributed to absence of a mechanism for emission of complex fragments below multifragmentation threshold in the SMM. The decrease of isoscaling parameter in the multifragmentation of target spectator at central collisions was reproduced using the simulation with spectator-participant model for dynamical stage and SMM for de-excitation stage. In all cases the isoscaling behavior was reproduced by proper description of the dynamical stage and no unambiguous signals on the decrease of the symmetry energy coefficient were observed.

The author acknowledges L. Tassan-Got for providing his DIT code and A.S. Botvina for providing his SMM code. This work was supported through grant of Slovak Scientific Grant Agency VEGA-2/5098/25.

## References

- [1] M. Veselsky, Fiz. Elem. Chastits At. Yadra 36, 400 (2005); Physics of Part. and Nuclei 36, 213 (2005).
- [2] M.B. Tsang et al., Phys. Rev. Lett. 2001. V.86. P.5023.
- [3] A.S. Botvina et al., Phys. Rev. C. 2002. V.65. P.44610.
- [4] O.V. Lozhkin, W. Trautmann, Phys. Rev. C. 1992. V.46. P.1996.
- [5] G.A. Souliotis et al., Phys. Rev. C. 2003. V.68. P.24605.
- [6] M. Veselsky, G.A. Souliotis, M. Jandel, Phys. Rev. C. 2004. V.69. P.44607.
- [7] J.P. Bondorf et al., Phys. Rep. 1995. V.257. P.133.
- [8] M. Veselsky, G.A. Souliotis, Nucl. Phys. A 765 (2006) 252.
- [9] M. Veselsky et al., Nucl. Phys. A. 2003. V.724. P.431.
- [10] M. Veselsky et al., Phys. Rev. C. 2000. V.62. P.064613.
- [11] L. Tassan-Got, PhD Thesis, 1988, Orsay, France, IPNO-T-89-02, 1989; L. Tassan-Got, C. Stéfan, Nucl. Phys. A. 1991. V.524. P.121.
- [12] M. Veselsky, G.A. Souliotis, S.J. Yennello, Phys. Rev. C. 2004. V.69. P.31603(R).
- [13] M. Veselsky, S.J. Yennello, Nucl. Phys. A 749, 114c (2005).
- [14] G.A. Souliotis et al., Phys. Lett. B. 2004. V.588. P.35.
- [15] G.A. Souliotis et al., Phys. Rev. Lett. 91 (2003) 022701.
- [16] M. Veselsky, G.A. Souliotis, arxiv.org:nucl-th/0607032.
- [17] A. Le Fevre et al., Phys. Rev. Lett. 94, 162701 (2005).
- [18] J. Gosset *et al.*, Phys. Rev. C **16** (1977) 629.
- [19] W.A. Friedman, Phys. Rev. C **27** (1983) 569.

- [20] J.-J. Gaimard, K.-H. Schmidt, Nucl. Phys. **A 531** (1991) 709.
- [21] K.-H. Schmidt et al., Phys. Lett. **B 300** (1993) 313.